A study of two-dimensional single atom-supported MXenes as hydrogen evolution reaction catalysts using DFT and machine learning

Hongxing Liang*, ***, Min Xu*, and Edouard Asselin*

*Department of Materials Engineering, The University of British Columbia, Vancouver, BC, Canada.

***Corresponding author: (001)6047739849

Department of Materials Engineering, The University of British Columbia, Frank Forward Building, 309-6350 Stores Road, Vancouver, BC, Canada, V6T 1Z4.

Email: hongxingliang314@gmail.com

Abstract

Screening promising hydrogen evolution reaction (HER) electrocatalysts for water splitting is crucial for the industrial scalability of sustainable energy storage. As HER catalysts, two-dimensional (2D) MXenes are promising substitution materials for platinum. Tuning the surface termination and loading a single atom can help improve the electrocatalytic performance of 2D MXenes. We utilized density functional theory (DFT) calculations to explore the catalyst activity and thermal stability of 2D single atom-loaded MXenes with surface terminations. We demonstrate that 21 uninvestigated 2D single-atom MXene catalysts, among 264 promising candidates, show an electrocatalytic activity surpassing that of platinum. Furthermore, machine learning tools predicted the catalyst activity and thermal stability using elemental properties that are easily available in chemical data repositories. The combination of DFT calculation and machine learning, as an advanced research strategy, shows promise for assessing a wide variety of HER electrocatalysts and screening new candidates with superior performance to metal platinum.

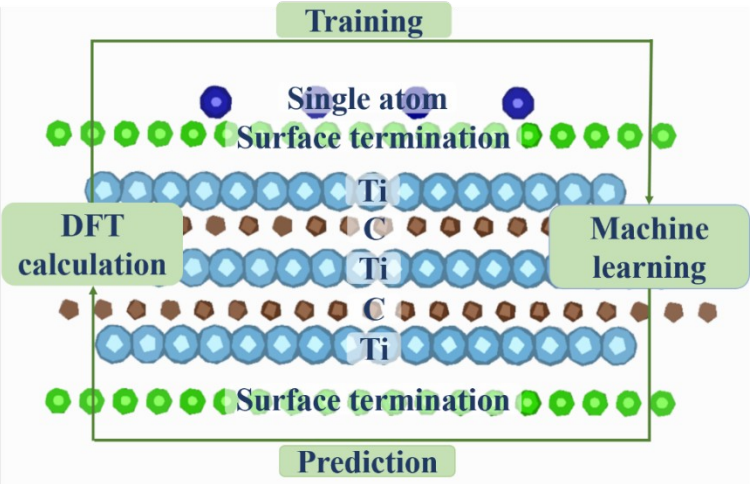

(Figure for Abstract)

1. Introduction

Research in the area of sustainable energy (e.g. solar and wind energy) is of continued and paramount importance.[1] Harvested solar and wind energy needs to be stored efficiently due to the discontinuous and variable nature of these energy sources.[2] Water splitting can be used to convert the discontinuous solar/wind energy into chemical energy where hydrogen gas is produced.[3] Catalysis of the HER is vital for the overall process efficiency of water splitting.[3] Further, the industrial scalability of hydrogen production from water splitting requires cost reductions such that the process may compete, on a cost basis, with hydrogen produced from fossil fuels.[4] One way to achieve process cost reductions is to replace the conventional and expensive platinum group metal catalysts with cheaper HER materials.[5]

2D MXenes have been widely researched as HER catalysts to replace platinum group metals due to their high electrical conductivity (4600 ± 1100 S/cm [6]), large active surface area (21 m^2/g [7]), and high stability in acidic electrolytes (MXenes can survive in hydrofluoric acid [8]). The chemical formula of MXenes is $M_{n+1}X_nT_x$(n=1, 2, 3) with M being a transition metal, X being C or N, and T representing the surface group (e.g. −O and −F).[9] The tuning of M (alloying), X, and T (surface functionalization) in $M_{n+1}X_nT_x$ has previously been carried out to improve the HER activity of 2D MXenes.[10] For instance, via tuning of the M in $M_{n+1}X_nT_x$, Wang et al. have used density functional theory (DFT) calculations to screen 2D $M_{n+1}X_nO_2$, $M_2M'X_2O_2$, and $M_2M'_2X_3O_2$ where M′ represents the transition metal. These authors found 110 unexplored structures with better HER activity than platinum group metals.[11] By tuning the X (from C to B) in $M_{n+1}X_n$, Sun et al. [12] utilized DFT calculations to screen Co/Ni_2B_2, Pt/Ni_2B_2, Co_2B_2, Os/Co_2B_2, and Mn/Co_2B_2 from 271 different structures with these 5 screened structures showing HER activity surpassing that of noble metal platinum. Wang et al. [13] indicated that surface functionalization (doping P region elements) improves the HER performance, resulting in a lower HER Gibbs free energy ($|\Delta G_H| < 0.2$ eV, absolute value) compared with that (0.2 eV) without surface functionalization. Kamysbayev et al. [14] have successfully synthesized MXenes with tellurium, bromine, selenium, sulfur, oxygen, imido, chlorine, and NH surface terminations by performing substitution and elimination reactions in molten inorganic salts without studying the HER catalytic activity of these structures. To the best of our knowledge, 2D MXenes with different terminations (e.g. bromine, imido, selenium, tellurium, boron, silicon, phosphorus, and NH) have not yet been investigated for the purposes of HER catalysis.

Single-atom catalysts immobilized on supports have attracted intense interest due to the high atom-utilization efficiency (a maximum efficiency of 100% [15]) and reduced content of noble metals (usually less than 1 wt % [16]). These materials have improved catalytic activity by enhancing the adsorption of reaction intermediates.[17] The MXenes with surface terminations are considered to be excellent electronic conductors and superior candidates for the support of single-atoms that facilitate the HER.[14] For instance, single-atom ruthenium sites supported on nitrogen-doped $Ti_3C_2T_x$ show superior HER activity with an $|\Delta G_H|$ of 0.039 eV,[18] which is closer to zero than that (0.09 eV) of Pt(111).[19, 20]

Inspired by the surface functionalization of MXenes and the advantages of single-atom catalysts, we examined the HER activity and thermal stability of 2D single atom-supported MXenes with surface terminations through DFT calculations to speed up the exploration of promising new HER catalysts. It is indicated in this work that 21 experimentally uninvestigated 2D single atom-supported MXenes with various surface terminations showed an electrocatalytic performance surpassing platinum. Additionally, we identified the important factors that govern the HER activity and thermal stability by machine learning, which accurately predicts the Gibbs free energy of hydrogen adsorption (reflecting activity [20]) and the cohesive energy (a proxy for thermal stability [21]). These important factors for Gibbs free energy and cohesive energy consist of 31 and 12, respectively, fundamental properties of elements (e.g. molar volume of surface element and the atomic radius of the surface element). This study not only provides promising HER catalysts that may replace noble metal platinum but also gives a machine learning algorithm for facile and accurate prediction of catalyst performance using only simple elemental properties.

2. Computational details

2.1. DFT details

DFT calculations were conducted using open-source Quantum-ESPRESSO [22, 23] with the Perdew–Burke–Ernzerhof (PBE) [24] exchange-correlation approximation. The nuclei–electron interaction was described using ultrasoft pseudopotentials.[25] Spin polarization was applied during DFT calculations. A plane wave basis with the energy cutoff of 769 eV was applied. Atomic positions were optimized until the forces were less than 0.01 eV/Å with the total energy converged to 1×10^{-4} eV. A k-mesh of 4 × 4 × 1 (for sampling the Brillouin zone) was utilized.[26] For single atoms anchored at the surface of MXenes, a 3×3×1 supercell was chosen with at least 18 Å vacuum space to avoid artificial interaction among the periodic units.

The Gibbs free energy of hydrogen adsorption (ΔG_H) was calculated to assess the HER activities of various catalysts calculated in this study based on the equation:[19, 20]

$$\Delta G_H = \Delta E_H + \Delta E_{ZPE}^H - T\Delta S_H$$

where ΔE_H (eV) is the total energy change before and after hydrogen adsorption, ΔE_{ZPE}^H (eV) represents the change in zero-point energy before and after hydrogen adsorption, T (K) is temperature and ΔS_H (J·mol^{-1} K^{-1}) is the difference in entropy between the adsorbed hydrogen atom and hydrogen gas. ΔE_H is obtained via the following equation:[19, 20]

$$\Delta E_H = \left(E_{nH^*} - E_{slab} - \frac{n}{2} E_{H_2} \right) / n$$

where E_{nH^*} (eV), E_{slab} (eV), and E_{H_2} (eV) are total energies (obtained from DFT calculation) of the catalyst with adsorbed nH atoms, the catalyst without adsorbed H atom, and isolated H_2 gas molecule, respectively. Furthermore, ΔE_{zPE}^H (eV) is expressed as:[19, 20]

$$\Delta E_{ZPE}^{H}=\left(E_{ZPE}^{nH}-\frac{n}{2}E_{ZPE}^{H_2}\right)/n$$

where ΔE_{ZPE}^{nH} (eV) and $E_{ZPE}^{H_2}$ are the zero-point energies (are based on the vibration frequency obtained from DFT calculation [27]) of the catalyst with adsorbed nH and isolated H_2 molecule, respectively. Finally, the following equation was used to calculate ΔS_H ($J \cdot mol^{-1}\ K^{-1}$):[19, 20]

$$\Delta S_H \cong -\frac{1}{2}S_{H_2}^{0}$$

where $S_{H_2}^{0}$ ($J \cdot mol^{-1}\ K^{-1}$) is the H_2 gas entropy under the standard condition.

In terms of cohesive energy, the following equation was used:[21, 28]

$$E_{coh}=E_{tot}\left(M_{n+1}X_nT_n-S\right)-(n+1)E_{atm}(M)-nE_{atm}(X)-nE_{atm}(T)-E_{atm}(S)$$

where E_{tot} (eV) and E_{atm} (eV) are the total energy of catalyst and the energies of free atoms of M, X, T as well as S (single atom), respectively. The cohesive energy per atom is further calculated in order to normalize the cohesive energy of different catalysts:[21, 28]

$$\acute{E}=E_{coh}/(n+1+n+n+1)$$

2.2. Machine learning methods

The machine learning calculations were conducted using Anaconda (an open-source Python distribution platform) with the libraries of TensorFlow and scikit-learn. The machine learning calculation in this work has two parts: feature engineering and model prediction. Machine learning efficiently establishes the correlation between input data and output based on computer algorithms.[29]

2.2.1 Feature engineering

Initially, 49 features (e.g. the atomic radius of the surface element, the molar volume of surface element) that may influence the ΔG_H and $\acute{E}$ were considered (see Table S1 in supplementary information).[30] These 49 features are the primary features of elemental properties that are easily available in chemical repositories or the periodic table of elements.[11, 12] The Pearson correlation coefficient was then calculated to select the non-linear dependence features. One of the two features is removed from feature groups when they show a high Pearson correlation coefficient (> 0.9).[12] Then the feature importance of each feature was obtained using random forestry (RFR) with the unimportant (≤0.001) features deleted.[12]

2.2.2 Model prediction

The features selected in Section 2.2.1 were used as input with the calculated ΔG_H and $\acute{E}$ data as output (see Table S1 in supplementary information). All catalysts examined in this work were further randomly separated into the training set and test set with a ratio of 7:3. To avoid a large variation in numerical values, a standardization of the dataset was applied to ensure that the feature values are centered at the mean value of 0 with the standard deviation of 1.[31] Then we utilized six different machine learning algorithms to

train the data, including artificial neural network (ANN), RFR, support vector regression (SVR), least absolute shrinkage and selection operator (LASSO), k-nearest neighbors (KNN), and Bayesian.[12, 32, 33] 10-fold cross-validations were conducted for all six algorithms to select the hyperparameter using the training data.[34] Then the algorithm parameters obtained from the training set were used to predict ΔG_H and $\acute{E}$ in the test set. The accuracy of each algorithm was assessed by the root mean square error (RMSE).

3. Results

3.1 Screening potential HER catalysis

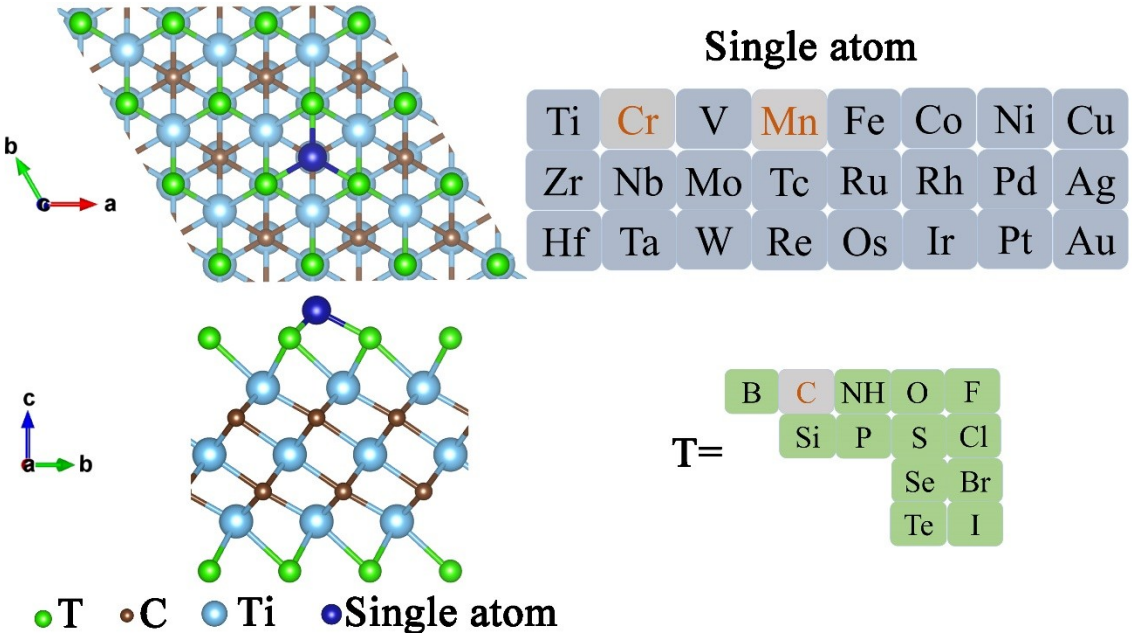

Fig. 1. Optimized atomic structure of single atom-loaded MXenes with surface termination elements and single atom elements. Cr and Mn were not considered for the single atom position, while C was not considered for the surface termination position.

The $Ti_3C_2T_2$ structure, one of most typical and widely studied MXenes, was selected in this work.[35] Based on previous studies,[14, 35, 36] the stable configuration of $Ti_3C_2T_2$ without the loaded single atoms is illustrated in Fig. S1 (see supplementary information) with all the functional groups (T= B, NH, O, F, Si, P, S, Cl, Se, Br, Te, and I) located on top of Ti in the third layer of atoms. To confirm this configuration, we also conducted the DFT calculations to obtain the total energies for the structures with surface termination elements at fcc, top, hcp, and bridge sites (Fig. S1 in supplementary information).[37] The site with the most negative total energy represents the most stable anchoring site. All surface elements studied are most stable at fcc anchoring sites (Table S1 in supplementary information). Further, previous studies [38, 39] have demonstrated that the single atom loaded on $Ti_3C_2T_2$ is located at the top of the C atom in the third atomic layer, and therefore that is what shown in Fig. 1. Cr and Mn were not considered for the single atom position due to the catalytically inactive nature of these two elements and the high

difficulty in structure convergence during the DFT calculations.[40] Finally, 12 surface termination element candidates coupled with the 22 single atom candidates lead to a total of 264 different structures.

$|\Delta G_H|$ for hydrogen adsorption is a well-established descriptor for the HER activity of catalysts,[41] thus H adsorption on the different structures studied in this work was examined using DFT computations. A highly negative ΔG_H corresponds to difficulty in H_2 desorption with a highly positive ΔG_H reflecting a large barrier to the electrochemical reduction reaction.[20] In literature, a catalyst is considered as an excellent candidate if it shows a value of $|\Delta G_H|$ smaller than 0.2 eV.[42] $|\Delta G_H|$ of Pt(111) is 0.09 eV.[20] The $|\Delta G_H|$ values for $Ti_3C_2T_2$ (T = B, O, I, P, S, Si, Br, F, Cl, Se, Te, and NH) without single atom loading are all above 0.2 eV with the smallest $|\Delta G_H|$ value of 0.5 eV for $Ti_3C_2Si_2$ and the largest $|\Delta G_H|$ value of 3.4 eV for $Ti_3C_2F_2$ (see Fig. S2 in supplementary information). The variation of surface termination of 2D MXenes resulted in a change in the $|\Delta G_H|$ value, further demonstrating the importance of surface tuning of 2D MXenes for HER catalysis.

As indicated in the introduction, 2D MXenes could be promising supports for single atoms. Through single-atom loading, the MXenes and dopant may produce more active-sites and thus enhance their HER performance.[43] Previous studies [18, 28, 43, 44] predominantly focused on the calculation of $|\Delta G_H|$ values of oxygen-terminated MXenes with single-atom loading as HER catalysts. However, we considered the combined effect of the 12 different surface terminations and single atom loading in the current study. Fig. 2 gives the $|\Delta G_H|$ values of 264 catalysts calculated in this work. After the loading of single atoms, 61 promising candidates among 264 calculated structures show excellent HER catalyst activity with $|\Delta G_H|$ values less than 0.2 eV. Further, 21 structures may have catalytic activity surpassing that of Pt (111) with $|\Delta G_H|$ values less than 0.09 eV. Importantly, these 21 structures have not previously been reported as HER catalysts (to the best of our knowledge) – these include: $Ti_3C_2B_2$−Re, $Ti_3C_2B_2$−Os, $Ti_3C_2B_2$−Ir, $Ti_3C_2O_2$−Re, $Ti_3C_2O_2$−Ir, $Ti_3C_2I_2$−Ir, $Ti_3C_2P_2$−Hf, $Ti_3C_2S_2$−Ti, $Ti_3C_2S_2$−Tc, $Ti_3C_2S_2$−Ir, $Ti_3C_2Si_2$−W, $Ti_3C_2Si_2$−Re, $Ti_3C_2Br_2$−Cu, $Ti_3C_2Br_2$−Pt, $Ti_3C_2F_2$−Ti, $Ti_3C_2F_2$−Fe, $Ti_3C_2F_2$−Ir, $Ti_3C_2Cl_2$−Cu, $Ti_3C_2Cl_2$−Pt, $Ti_3C_2Se_2$−Au, and $Ti_3C_2Te_2$−Nb.

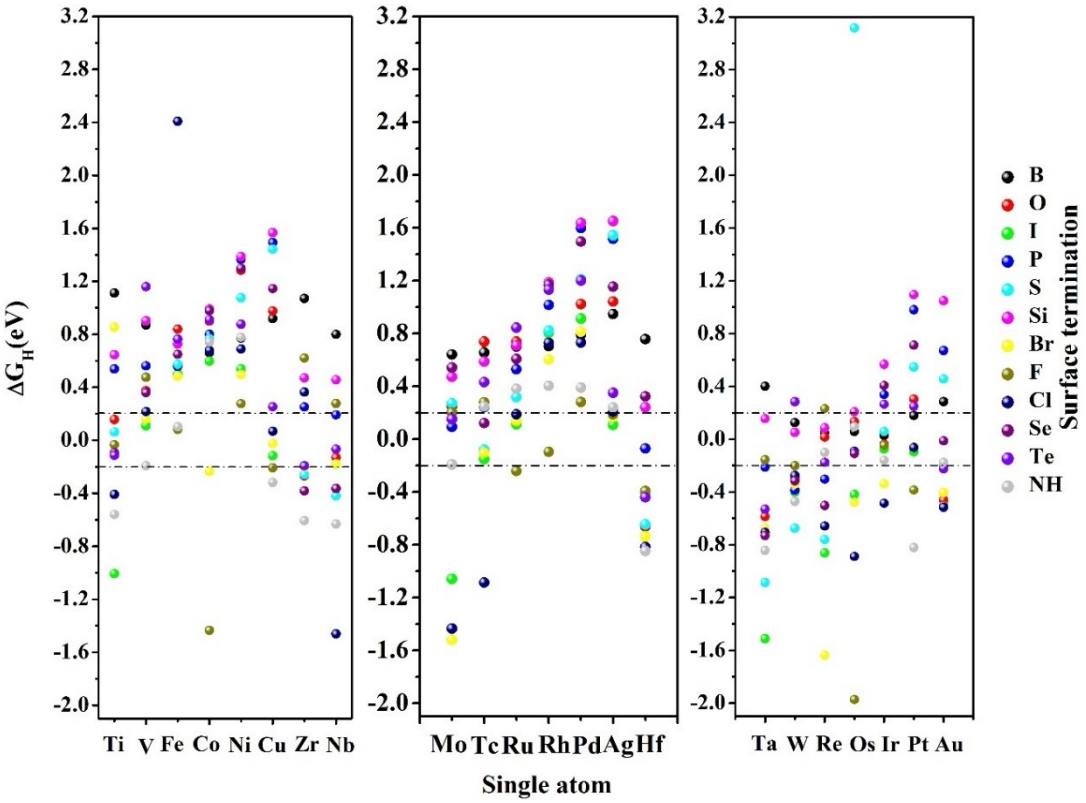

Fig. 2 The Gibbs free energy (ΔG_H) distributions of hydrogen adsorbed on different 2D single atom-loaded MXenes. The upper and lower dashed lines in Fig. 2 correspond to the values of 0.2 eV and −0.2 eV, respectively.

The experimental feasibility (or the thermal stability) of DFT calculated 2D materials is usually evaluated by its cohesive energy per atom with a higher absolute value corresponding to higher stability.[21] The absolute cohesive energies for all the structures (264 in total) studied in this work are in the range of 5.9 to 8 eV/atom (Fig. 3), which are higher than those of synthesized borophene sheet (5.81 eV/atom) and MoS_2 (5.02 eV/atom),[45] indicating that all studied structures in this work show higher experimental feasibility. The variation in cohesive energies of the MXenes with and without (see Fig. S3 in supplementary information) single atoms are less than 0.2 eV, indicating that the loading of the single atom does not significantly influence the thermal stability of the MXenes. As shown in Fig. 3, the O (~7.9 eV) and F (~7.1 eV) terminated structures show higher thermal stability, whereas the I terminated structures have the lowest thermal stability (~5.9 eV). This coincides with the fact that the experimentally prepared MXenes are generally terminated with O and F groups [46] and provides theoretical support to this fact. Notably, the thermal stability (Fig. 4) of the 21 promising HER candidates with catalytic activity surpassing Pt (111) are within the range spanning $Ti_3C_2O_2$−Re (7.9 eV) and $Ti_3C_2I_2$−Ir (6.0 eV), showing the highest and lowest stability, respectively.

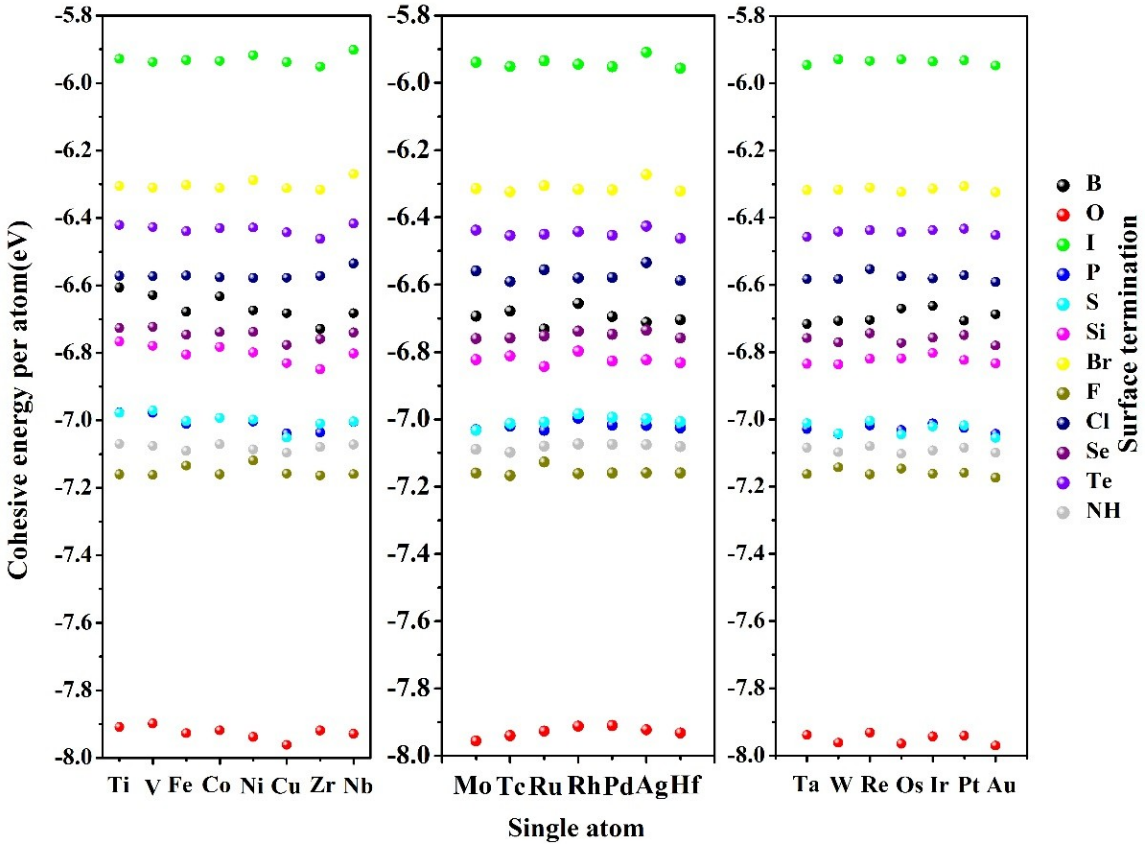

Fig. 3 Cohesive energy distributions of hydrogen adsorbed on different 2D single atom-loaded MXenes.

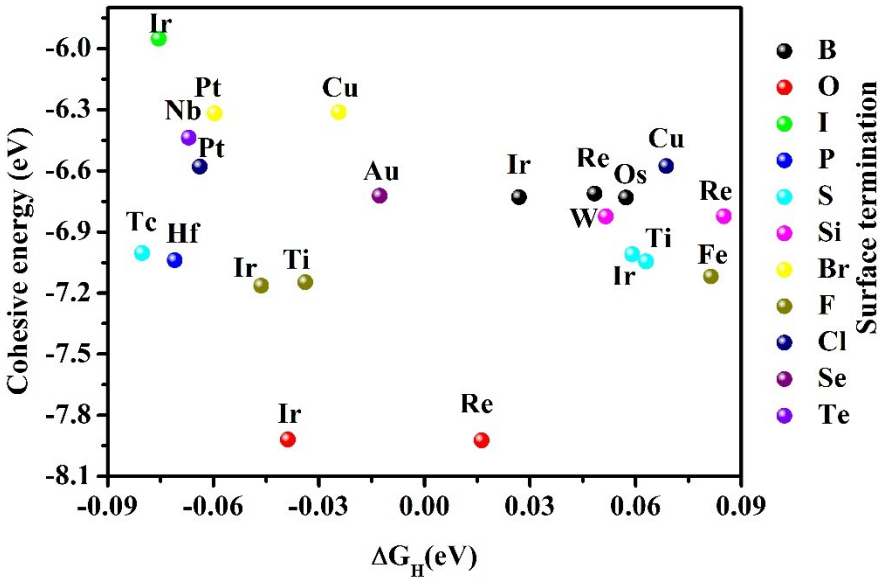

Fig. 4 The Gibbs free energy and cohesive energy of 21 promising catalysts ($Ti_3C_2T_x$ with single atom loaded) which may show better catalytic activity with respect to Pt(111).

The change of ΔG_H and $\acute{E}$ with the variation of surface termination and single atom choice cannot be expressed by a simple linear relationship. The key factors that influence the ΔG_H and $\acute{E}$ values of the 2D single atom-loaded MXenes need to be determined. To address this issue, a quantitative exploration of as-yet unknown data correlations is conducted via machine learning, which is becoming increasingly popular in the catalyst field.[47]

3.2 Feature engineering and model prediction by machine learning

The unknown correlation between inputs (various features) and outputs (ΔG_H and $\acute{E}$) established by machine learning was desirable for further ΔG_H and $\acute{E}$ predictions.[48] Additionally, recent investigations in the catalyst field have indicated that the screening of promising catalysts could be accelerated by machine-learning.[49] Unpromising candidates can be excluded by machine learning, thus reducing the number of DFT calculations.[50]

The quality of the various numerical features of different catalysts determines the model prediction of the machine learning algorithm. The published studies [51-53] about machine learning prediction in the catalyst field predominantly tended to use the electronic features of active surface atoms, including d-band characteristics and Bader charge transfer, which require further non-self-consistent field calculation. However, this requires ab initio level computational cost to prepare these features. Consequently, it is strongly desirable to develop machine learning algorithms that only utilize readily available data (e.g. easily found elemental properties) without using DFT-obtained features to achieve an efficient search over the broad catalyst group. In the meantime, the use of these more easily found features should not result in a significant loss in prediction accuracy.

In this work, 49 elemental properties (see Table S2 in the supplementary information) that are easily available in chemical repositories or the periodic table of elements were selected without using DFT-obtained features.[11, 12] Based on the correlation map of the 49 features by Pearson correlation coefficient (see Fig. S4 in the supplementary information), 17 features were removed from the feature group due to a high level of linear correlation. After that, 32 features remained, including the ionic radius of a single atom (labeled as IA), ionic radius of surface group element (IG), atom number of single atom (AA), first ionization potential of single atom (FA), second ionization potential of single atom (SA), third ionization potential of single atom (TA), first ionization potential of surface group element (FG), electron affinities of single atom (EA), electron affinities of surface element (EG), boiling point of single atom (BA), boiling point of surface element (BG), melting point of single atom (MA), Pauling electronegativity of single atom (PA), atomic radius of single atom (AR), charge transfer of single atom (CA), charge transfer of surface element (CG), crystal radius of single atom (CR), crystal radius of surface element (CS), atomic mass of surface element (AS), covalent radius of single atom (CO), molar volume of single atom (MV), molar volume of surface element (MS), group number in periodic table for single atom (GS), group number in periodic table for surface element (GG), nuclear spin of single atom in (NA), nuclear spin of surface

element (NG), thermal neutron capture of single atom (TA), thermal neutron capture of surface element (TG), effective nuclear charge of single atom at different orbit (EE), work function of single atom (WA), thermal conductivity of single atom at room temperature (TC), and thermal conductivity of surface element at room temperature (TS).

The importance of these 32 features for ΔG_H and $\acute{E}$ predictions are given in Fig. 5 (a and b). Fig. 5 (a) shows that the ΔG_H prediction is dependent on features of both surface elements and single atoms. This further indicates that the synergistic effect between the surface termination and single atom loading can affect the HER catalytic reactivity. This is due to the important role of surface groups in electron transfer and the affected intermediate adsorption and reaction kinetics as a result of surface functionalization.[38] For $\acute{E}$ prediction, the low importance features were further dropped with only 12 features (IG, FG, EG, BG, CG, CS, AS, MS, GG, NG, TG, and TS) kept to maintain the importance and precision simultaneously. Moreover, these 12 features kept for $\acute{E}$ prediction are all the properties of surface termination elements, indicating that the cohesive energy is predominantly dependent on the properties of surface termination elements. This also validates our proposal stated in the introduction to study the surface tuning effect of MXenes.

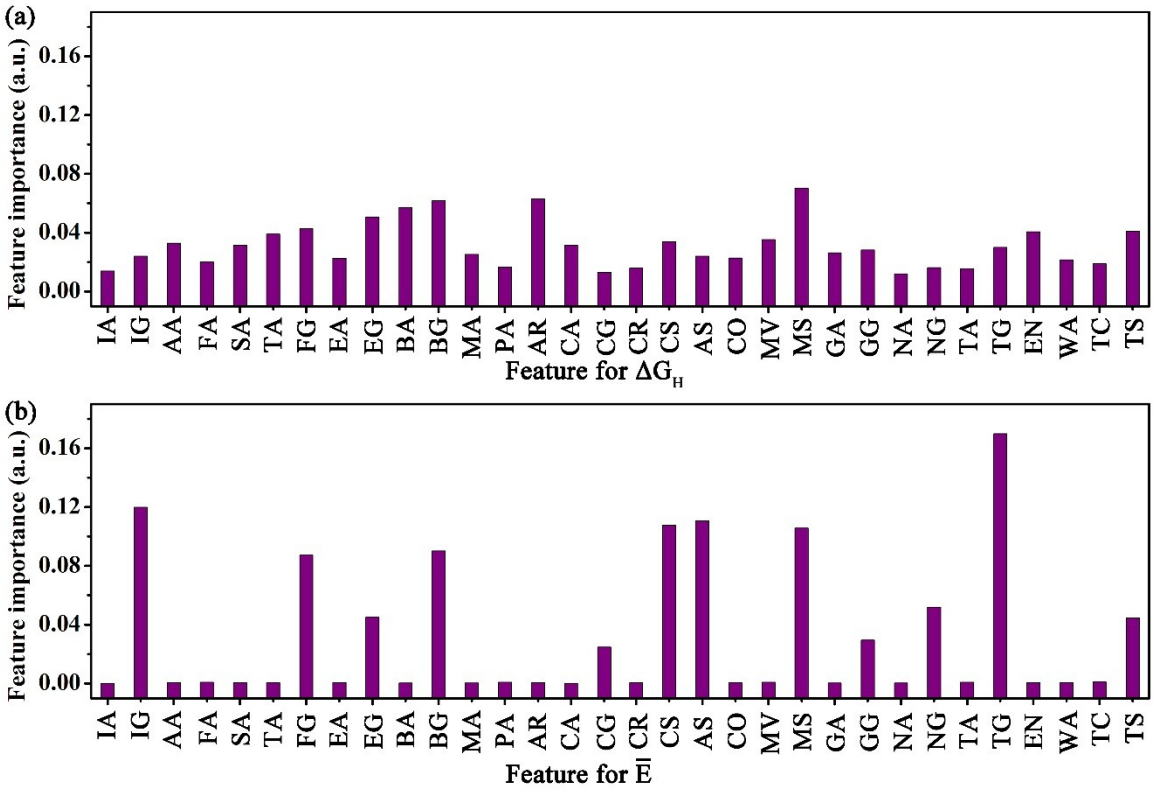

Fig. 5 Feature importance of 32 different features used for ΔG_H and $\acute{E}$ predictions.

Machine learning algorithms were employed to predict ΔG_H and $\acute{E}$, including ANN, RFR, SVR, LASSO, KNN, and Bayesian. Fig. 6 (a and b) presents the ANN-predicted values and DFT-calculated values with those values for other algorithms given in the supplementary information (Fig. S5−9). The testing set using ANN shows the RMSE of

0.158 eV and 0.04 eV for two-value predictions. ANN shows the lowest RMSE in the ΔG_H prediction, while RFR and KNN have the lowest RMSE (0.02 eV) in the $\acute{E}$ prediction (Fig. 6 (c and d)). ANN has many layers with each layer showing several neurons which would process the cumulative input from neurons of a previous layer via an activation function (a sigmoid function in this work).[54] A gradient descent optimization algorithm is used to systematically tune the weights connecting different neurons until convergence. The small variations in input can be responded by ANN without causing a change in output, thus ANN is more fault-tolerant.[55] We used the ANN consisting of two hidden layers with 3 and 3 neurons (learning rate is 0.005 with training epoch of 250) which shows the smallest prediction error (~0.158 eV) in ΔG_H prediction. For $\acute{E}$ prediction, though only 12 important features were kept, it is still achieved by an amazing low error (0.02 eV) using algorithms of RFR (the number of trees is 200 and the minimum number of samples required to split is 4) and KNN (the number of neighbors is 7).

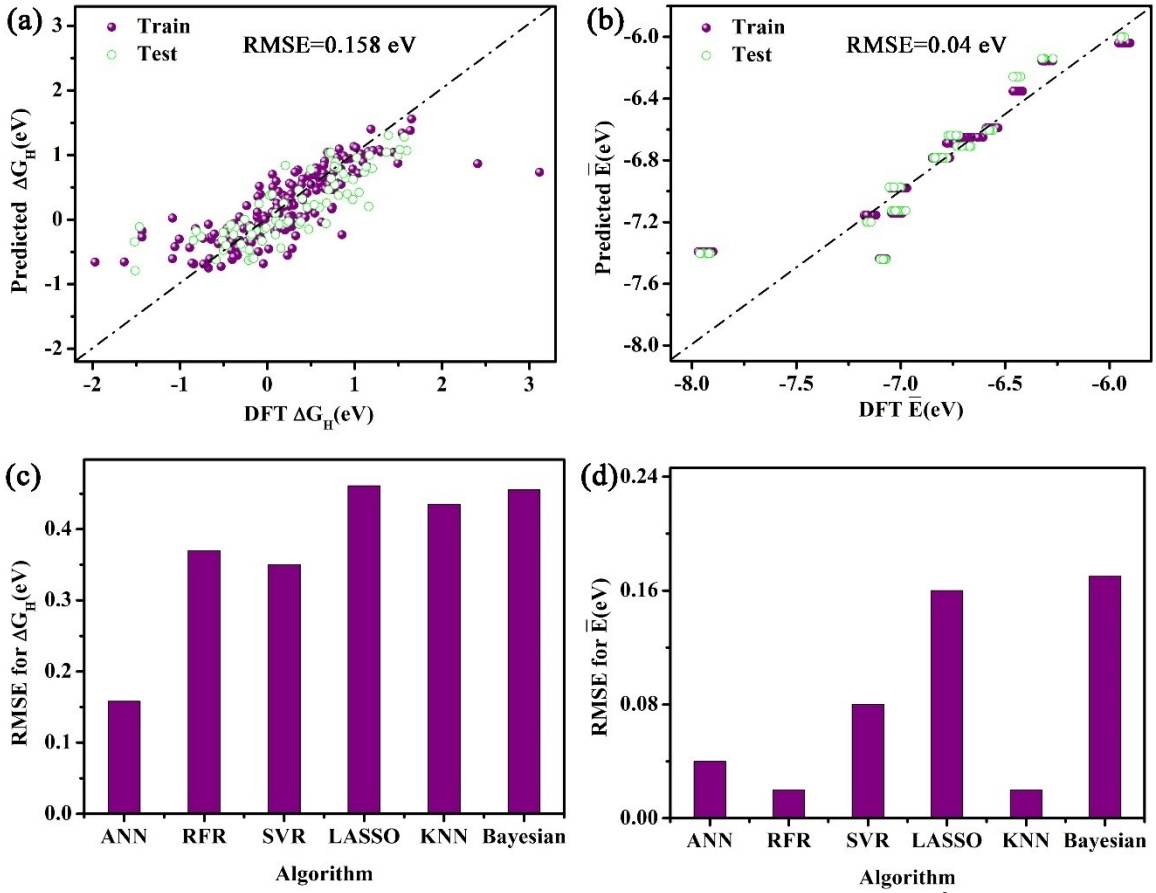

Fig. 6 The performance of ANN used for the prediction of ΔG_H (a) and $\acute{E}$ (b), as well as the RMSE for different algorithms used for prediction of ΔG_H (c) and $\acute{E}$ (d).

It has now been demonstrated that, only using elemental properties that are readily available, we are able to obtain a similar precision (RMSE of 0.158 eV) with those studies (0.15 eV,[12] 0.14 eV,[11] and 0.17 eV [56]) using the electronic features (e.g. d band center and Bader charge transfer) that need further non-self-consistent field calculation

associated with high computational cost. It should be noted that the cohesive energy of the single atom-loaded MXenes has not previously been predicted (to the best of our knowledge) by machine learning with such a low RMSE (0.02 eV). The direct comparison of the computational speeds for DFT calculation and machine learning is hard. An easy structural optimization (e.g. C_2Br_2−Pt) using DFT calculation would take 131.2 core-hour, while the slowest machine learning algorithm (that is ANN) would take 0.05 core-hour to achieve the model prediction of ΔG_H. Because of the faster calculation speed of machine learning in comparison to DFT calculation, the algorithms described in this work may help future researchers quickly screen single atom-loaded MXenes HER catalysts at the initial design stage. Then DFT calculation and laboratory experiments can be used to further screen the promising catalysts identified via machine learning.

4. Conclusions

The HER electrocatalytic performance of 2D MXenes can be controlled via the tuning of both surface termination and the loading of single atoms. Via DFT calculations, we have screened 61 ideal HER catalysts from 264 candidates of two-dimensional single atom-supported MXenes with terminations that may be experimentally prepared. Among the most promising HER catalysts, 21 showed better HER activity (with the $|\Delta G_H|$ values less than 0.09 eV) than that of Pt.

The HER electrocatalytic performance and thermal stability of the catalysts studied in this work were further supported by machine learning algorithms (ANN, RFR, SVR, LASSO, KNN, and Bayesian). Most importantly, we present a way to provide a comparable precision (RMSE values for the activity and thermal stability predictions are 0.158 eV and 0.02 eV, respectively) to the published machine learning works by avoiding their adoption of complex electronic features and the associated high computational cost, and by only using features that are easily available in chemical repositories. The algorithms used in this work are expected to help future researchers quickly screen single atom loaded MXenes HER catalysts at the initial design stage in a cost-effective manner.

Acknowledgements

The financial support from the Natural Sciences and Engineering Research Council of Canada (NSERC) is acknowledged. The corresponding author would like to express his gratitude to Dr. Zihe Ren of Jetti Services Canada and Dr. Jing Liu of the University of Alberta for many useful discussions about this work.

References

1. A. M. Omer, Renewable and Sustainable Energy Reviews, 2008, 12, 2265-2300.
2. S. E. Hosseini and M. A. Wahid, Renewable and Sustainable Energy Reviews, 2016, 57, 850-866.
3. H. Ahmad, S. Kamarudin, L. Minggu and M. Kassim, Renewable and Sustainable Energy Reviews, 2015, 43, 599-610.

4. P. Nikolaidis and A. Poullikkas, Renewable and Sustainable Energy Reviews, 2017, 67, 597-611.
5. J. Deng, P. Ren, D. Deng, L. Yu, F. Yang and X. Bao, Energy & Environmental Science, 2014, 7, 1919-1923.
6. A. Lipatov and A. Sinitskii, in 2D Metal Carbides and Nitrides (MXenes): Structure, Properties and Applications, eds. B. Anasori and Y. Gogotsi, Springer International Publishing, Cham, 2019, DOI: 10.1007/978-3-030-19026-2_16, pp. 301-325.
7. B. Wang, A. Zhou, F. Liu, J. Cao, L. Wang and Q. Hu, Journal of Advanced Ceramics, 2018, 7, 237-245.
8. P. Li, J. Zhu, A. D. Handoko, R. Zhang, H. Wang, D. Legut, X. Wen, Z. Fu, Z. W. Seh and Q. Zhang, Journal of Materials Chemistry A, 2018, 6, 4271-4278.
9. M. Naguib, V. N. Mochalin, M. W. Barsoum and Y. Gogotsi, Advanced Materials, 2014, 26, 992-1005.
10. X. Hui, X. Ge, R. Zhao, Z. Li and L. Yin, Advanced Functional Materials, 2020, 30, 2005190.
11. X. Wang, C. Wang, S. Ci, Y. Ma, T. Liu, L. Gao, P. Qian, C. Ji and Y. Su, Journal of Materials Chemistry A, 2020, 8, 23488-23497.
12. X. Sun, J. Zheng, Y. Gao, C. Qiu, Y. Yan, Z. Yao, S. Deng and J. Wang, Applied Surface Science, 2020, 526, 146522.
13. Y. Yoon, A. P. Tiwari, M. Choi, T. G. Novak, W. Song, H. Chang, T. Zyung, S. S. Lee, S. Jeon and K. S. An, Advanced Functional Materials, 2019, 29, 1903443.
14. V. Kamysbayev, A. S. Filatov, H. Hu, X. Rui, F. Lagunas, D. Wang, R. F. Klie and D. V. Talapin, Science, 2020, 369, 979-983.
15. L. Zhang, K. Doyle-Davis and X. Sun, Energy & Environmental Science, 2019, 12, 492-517.
16. J. Kim, H. E. Kim and H. Lee, ChemSusChem, 2018, 11, 104-113.
17. L. Cao, Q. Luo, W. Liu, Y. Lin, X. Liu, Y. Cao, W. Zhang, Y. Wu, J. Yang and T. Yao, Nature Catalysis, 2019, 2, 134-141.
18. H. Liu, Z. Hu, Q. Liu, P. Sun, Y. Wang, S. Chou, Z. Hu and Z. Zhang, Journal of Materials Chemistry A, 2020, 8, 24710-24717.
19. J. Rossmeisl, J. K. Nørskov, C. D. Taylor, M. J. Janik and M. Neurock, The Journal of Physical Chemistry B, 2006, 110, 21833-21839.
20. J. K. Nørskov, T. Bligaard, A. Logadottir, J. Kitchin, J. G. Chen, S. Pandelov and U. Stimming, Journal of The Electrochemical Society, 2005, 152, J23.
21. N. Zhang, Y. Hong, S. Yazdanparast and M. A. Zaeem, 2D Materials, 2018, 5, 045004.
22. P. Giannozzi, S. Baroni, N. Bonini, M. Calandra, R. Car, C. Cavazzoni, D. Ceresoli, G. L. Chiarotti, M. Cococcioni and I. Dabo, Journal of Physics: Condensed Matter, 2009, 21, 395502.
23. P. Giannozzi, O. Andreussi, T. Brumme, O. Bunau, M. B. Nardelli, M. Calandra, R. Car, C. Cavazzoni, D. Ceresoli and M. Cococcioni, Journal of Physics: Condensed Matter, 2017, 29, 465901.
24. J. P. Perdew, K. Burke and M. Ernzerhof, Physical Review Letters, 1996, 77, 3865.
25. K. F. Garrity, J. W. Bennett, K. M. Rabe and D. Vanderbilt, Computational Materials Science, 2014, 81, 446-452.
26. D. Chadi, Physical Review B, 1977, 16, 1746.

27. G. Gao, A. P. O'Mullane and A. Du, Acs Catalysis, 2017, 7, 494-500.
28. Z. Shen, X. Fan, S. Ma, Y. An, D. Yang, N. Guo, Z. Luo and Y. Hu, International Journal of Hydrogen Energy, 2020, 45, 14396-14406.
29. L. Ward, A. Agrawal, A. Choudhary and C. Wolverton, npj Computational Materials, 2016, 2, 1-7.
30. X. Wang, B. Xiao, Y. Li, Y. Tang, F. Liu, J. Chen and Y. Liu, Applied Surface Science, 2020, 531, 147323.
31. D. Singh and B. Singh, Applied Soft Computing, 2020, 97, 105524.
32. J.-C. Huang, K.-M. Ko, M.-H. Shu and B.-M. Hsu, Neural Computing and Applications, 2020, 32, 5461-5469.
33. N. J. O'Connor, A. Jonayat, M. J. Janik and T. P. Senftle, Nature Catalysis, 2018, 1, 531-539.
34. P. Probst, A.-L. Boulesteix and B. Bischl, Journal of Machine Learning Research, 2019, 20, 1-32.
35. T. Schultz, N. C. Frey, K. Hantanasirisakul, S. Park, S. J. May, V. B. Shenoy, Y. Gogotsi and N. Koch, Chemistry of Materials, 2019, 31, 6590-6597.
36. Y. Bai, K. Zhou, N. Srikanth, J. H. Pang, X. He and R. Wang, RSC Advances, 2016, 6, 35731-35739.
37. B. Ding, W.-J. Ong, J. Jiang, X. Chen and N. Li, Applied Surface Science, 2020, 500, 143987.
38. Q. Peng, J. Zhou, J. Chen, T. Zhang and Z. Sun, Journal of Materials Chemistry A, 2019, 7, 26062-26070.
39. Y. Gao, H. Zhuo, Y. Cao, X. Sun, G. Zhuang, S. Deng, X. Zhong, Z. Wei and J. Wang, Chinese Journal of Catalysis, 2019, 40, 152-159.
40. S. Anantharaj, H. Sugime and S. Noda, ACS Applied Energy Materials, 2020, 3, 12596-12606.
41. V. Fung, G. Hu, Z. Wu and D.-e. Jiang, The Journal of Physical Chemistry C, 2020, 124, 19571-19578.
42. C. Ling, L. Shi, Y. Ouyang and J. Wang, Chemistry of Materials, 2016, 28, 9026-9032.
43. J. Zhang, Y. Zhao, X. Guo, C. Chen, C.-L. Dong, R.-S. Liu, C.-P. Han, Y. Li, Y. Gogotsi and G. Wang, Nature Catalysis, 2018, 1, 985-992.
44. X. Yang, Z. Lu, C. Cheng, Y. Wang, X. Zhang, Z. Yang and W. Lu, The Journal of Physical Chemistry C, 2020, 124, 4090-4100.
45. Z. Jiang, P. Wang, X. Jiang and J. Zhao, Nanoscale Horizons, 2018, 3, 335-341.
46. M. Naguib, O. Mashtalir, J. Carle, V. Presser, J. Lu, L. Hultman, Y. Gogotsi and M. W. Barsoum, ACS Nano, 2012, 6, 1322-1331.
47. J. Schmidt, M. R. Marques, S. Botti and M. A. Marques, npj Computational Materials, 2019, 5, 1-36.
48. J. Schmidt, M. R. G. Marques, S. Botti and M. A. L. Marques, npj Computational Materials, 2019, 5, 83.
49. B. R. Goldsmith, J. Esterhuizen, J. X. Liu, C. J. Bartel and C. Sutton, AIChE Journal, 2018, 64, 2311-2323.
50. K. Tran and Z. W. Ulissi, Nature Catalysis, 2018, 1, 696-703.
51. Z. Li, S. Wang, W. S. Chin, L. E. Achenie and H. Xin, Journal of Materials Chemistry A, 2017, 5, 24131-24138.

52. Z. Li, X. Ma and H. Xin, Catalysis Today, 2017, 280, 232-238.
53. Z. Yang, W. Gao and Q. Jiang, Journal of Materials Chemistry A, 2020, 8, 17507-17515.
54. S. Sharma, International Journal of Engineering Applied Sciences and Technology, 2020, 4, 310-316.
55. C. Torres-Huitzil and B. Girau, IEEE Access, 2017, 5, 17322-17341.
56. J. Zheng, X. Sun, C. Qiu, Y. Yan, Z. Yao, S. Deng, X. Zhong, G. Zhuang, Z. Wei and J. Wang, The Journal of Physical Chemistry C, 2020, 124, 13695-13705.